

## 폴리비닐 클로라이드의 광안정성 향상을 위한 세륨 및 사마륨 산화물 도입

Ali Jabbar A. Al-Sarray<sup>†</sup>, Basma Esam Jasim\*, Nibras Abdul-Ameer Aboud\*, and Fatimah Jumaah Moaen

Polymer Research Unit, College of Science, Mustansiriyah University

\*Department of Chemical Industrial, Institute of Technology/Baghdad, Middle Technical University

(2023년 10월 20일 접수, 2024년 1월 21일 수정, 2024년 1월 21일 채택)

## Enhancing the Photostability of Poly(Vinyl Chloride) (PVC) Through the Incorporation of Cerium and Samarium Oxide

Ali Jabbar A. Al-Sarray<sup>†</sup>, Basma Esam Jasim\*, Nibras Abdul-Ameer Aboud\*, and Fatimah Jumaah Moaen

Polymer Research Unit, College of Science, Mustansiriyah University, 10052 Iraq

\*Department of Chemical Industrial, Institute of Technology/Baghdad, Middle Technical University, 10074 Iraq

(Received October 20, 2023; Revised January 21, 2024; Accepted January 21, 2024)

**Abstract:** This study focuses on enhancing the photostability of poly(vinyl chloride) (PVC) by incorporating it with a nanocomposite ( $\text{CeO}_2/\text{Sm}_2\text{O}_3$ ) synthesized through a chemical method. The nanocomposite's characteristics, including the crystallite size (21.23 nm), grain size (27 nm by field emission scanning electron microscope, 23 nm by transmission electron microscope), and X-ray diffractometer analysis, were investigated. Thin PVC films with and without the nanocomposite were fabricated and analyzed for optical and morphological properties using Fourier-transform infrared spectroscopy and atomic force microscopy. Photostability was assessed through indices ( $I_{\text{CO}}$ ,  $I_{\text{PO}}$ ,  $I_{\text{OH}}$ ), weight loss measurements after UV radiation exposure. Results indicate a noticeable reduction in PVC film decomposition, showcasing the nanocomposites' potential as effective light stabilizers. AFM and microscopic analyses further support the stabilizing efficiency. This research contributes valuable insights into utilizing  $\text{CeO}_2/\text{Sm}_2\text{O}_3$  nanocomposites for enhancing PVC photostability.

**Keywords:** poly(vinyl chloride),  $\text{CeO}_2/\text{Sm}_2\text{O}_3$  nanocomposite, roughness, photo degradation, photostability.

### Introduction

Poly(vinyl chloride) (PVC) is one of the widely used and adapted thermoplastic materials due to insulating the electricity, resisting the weathering, possessing excellent aesthetic quality, and being durable.<sup>1</sup> Being the building block of producing medical and sport equipments, clothes, construction materials, packaging, and electronic devices, PVC is one of the highly demanded materials from the industrial perspective in order to meet the increasing global requirement.<sup>2-4</sup> However, the inherent thermal instability of PVC, stemming from structural weaknesses within the polymer chain, such as allyl chloride, tertiary chloride, and carbonyl allyl chloride, poses chal-

lenges during thermal processing.<sup>5-7</sup>

Exposing PVC to high temperature and ultraviolet radiation accompanied by environmental oxygen, causes chemical and physical alternations, including dehydrochlorination process, which are undesirable.<sup>8,9</sup> Releasing hydrochloric acid (HCl) induces the formation of polyene, hydroxy, and carbonyl residues,<sup>10</sup> which initiates the formation of free radical that accelerate the degradation process of PVC.<sup>11,12</sup> To address this issue, thermal stabilizers like layered hydrotalcite compounds, liquid mixed metals, metal soaps, and organic tin/lead salts have been historically employed to prevent thermal degradation during PVC production.<sup>13</sup> The environmental concerns associated with lead-based and organotin compound stabilizers have prompted significant research into developing non-toxic alternatives.<sup>14,15</sup>

In recent years, rare earth compounds have gained attention as potential PVC thermal stabilizers, with examples including lanthanum cyanurate,<sup>16</sup> lanthanum-pentaerythritol alkoxide,<sup>17</sup>

<sup>#</sup>These authors equally contributed to this work.

<sup>†</sup>To whom correspondence should be addressed.

ali\_alsarray@uomustansiriyah.edu.iq, ORCID<sup>®</sup> 0000-0001-6484-1763

©2024 The Polymer Society of Korea. All rights reserved.

lanthanum histidine,<sup>16</sup> and lanthanum sulfadiazine.<sup>3</sup> These stabilizers have exhibited the ability to modify PVC conformation, inhibit dehydrochlorination, and replace unstable chlorine in PVC chains, ultimately impeding the chain reaction and catalysis by HCl, thereby stabilizing the material.<sup>14,15</sup>

Among these materials, cerium oxide nanoparticles ( $\text{CeO}_2$ ) have emerged as promising candidates for PVC stabilization due to their compatibility with the binary transition state.<sup>18</sup>  $\text{CeO}_2$  stands out as a versatile material with multifaceted utility, characterized by its excellent thermal stability at elevated temperatures, abundance of oxygen vacancies on its surface, substantial specific area facilitating Faradaic processes, superior mechanical strength, and enhanced electron transmission.<sup>19,20</sup> Furthermore, when combined with metals, either as composites or through doping,  $\text{CeO}_2$ 's properties are further enhanced, including its oxygen storage capacity.<sup>19</sup> This versatile compound, thanks to its  $4f^1$  valence state and presence of  $\text{Ce}^{3+}$  and  $\text{Ce}^{4+}$  oxidation states, also exhibits exceptional recyclability, high retention rates, cost-effectiveness, reduced toxicity, regulated pore size, a favorable environmental profile, improved catalytic properties, and rapid redox reactivity.<sup>21</sup>

Similarly, samarium (Sm), a member of the lanthanide group, offers a range of oxidation states, enabling its use in a wide spectrum of applications, including optical lasers, supercapacitors, solar cells, biochemical sensors, nanoelectronics, and photocatalysts.<sup>22,23</sup> The synergistic effects of binary metal oxides render them more advantageous in terms of specific capacity and electrochemical characteristics compared to their single-metal counterparts. Various synthesis methods, such as co-precipitation, hydrothermal, sol-gel, chemical vapor deposition, and electro-deposition, have been employed to produce nanoparticles, with hydrothermal techniques being particularly versatile and cost-effective, yielding a variety of nanostructures.<sup>21</sup>

Nevertheless, research into rare earth stabilizers has been relatively limited, constrained by challenging manufacturing processes, low yield, and inconsistent performance.<sup>24-26</sup> Therefore, a comprehensive understanding of rare earth thermal stabilizers is essential to leverage the potential benefits of rare earth materials effectively. The aim of the present work is to investigate the stabilization ability of cerium oxide and samarium oxide nanoparticles when integrated with PVC.

## Experimental

**Instruments.** The experimental work was conducted utilizing the following equipment and instruments: a Companion

BS-11, a KERN-ABS digital scale, a CARY 100 Conc UV–visible spectrometer, a Philips XL series 30 Field Emission Scanning Electron Microscope (FE-SEM), a Shimadzu 8400 Fourier-transform infrared spectrometer (FTIR), and a Shimadzu-XRD 6000 X-ray diffractometer.

**Materials.** Cerium nitrate hexahydrate ( $\text{Ce}(\text{NO}_3)_3 \cdot 6\text{H}_2\text{O}$ ), samarium (III) nitrate hexahydrate ( $\text{Sm}(\text{NO}_3)_3 \cdot 6\text{H}_2\text{O}$ ), urea ( $\text{CH}_4\text{N}_2\text{O}$ ), and tetrahydrofuran (THF) were procured from Merck, Ltd. whereas PVC with about 233000 g/mol of average molecular weight and 800 degree of polymerization purchased from Petkim Petrokimya (Turkey) and were used without further purification.

**Preparation of  $\text{CeO}_2/\text{Sm}_2\text{O}_3$  Nanocomposites.** The nanocomposite was synthesized *via* a chemical process involving the salts  $\text{Sm}(\text{NO}_3)_3 \cdot 6\text{H}_2\text{O}$  and  $\text{Ce}(\text{NO}_3)_3 \cdot 6\text{H}_2\text{O}$ . An aqueous solution of  $\text{Ce}(\text{NO}_3)_3 \cdot 6\text{H}_2\text{O}$ ,  $\text{Sm}(\text{NO}_3)_3 \cdot 6\text{H}_2\text{O}$ , and urea was prepared at a concentration of 0.5 mol. Sodium hydroxide (NaOH) solution was added dropwise at room temperature and stirred for 3 hours. Subsequently, the mixture was concentrated, washed multiple times with deionized water, and then subjected to drying. The produced composite was heated to 80 °C, which caused it to participate, and then calcined at 500 °C for 3 hours, producing a yellowish-white colored powder.

**Preparation of Thin Film Nanocomposites of PVC and  $\text{CeO}_2/\text{Sm}_2\text{O}_3$ .** The preparation of the thin films of PVC with  $\text{CeO}_2/\text{Sm}_2\text{O}_3$  nanocomposites was carried out in two stages. In the first stage, a pure PVC thin film was prepared by mixing 1 g of PVC with 100 mL of THF to form a 1% weight mixture, which was then stirred and heated to 75 °C before being cast into a glass mold. In the second stage, 0.05 g of the  $\text{CeO}_2/\text{Sm}_2\text{O}_3$  nanocomposite material was incorporated into the PVC mixture, thoroughly mixed using a stirrer, and subsequently subjected to ultrasonication for 30 min to remove air bubbles and aid in the dissolution of the nanocomposite material. The resulting nanocomposite films were then cast into 40  $\mu\text{m}$  glass templates and allowed to dry under vacuum conditions in circular glass molds. The films were exposed to UV light at  $6.0 \times 10^{-9}$   $\text{ein} \cdot \text{dm}^{-3} \cdot \text{S}^{-1}$  with a  $\lambda_{\text{max}}$  of 313 nm for 50-300 h, with occasional turning for even exposure.

## Results and Discussion

**X-ray Diffraction Patterns of the  $\text{CeO}_2/\text{Sm}_2\text{O}_3$  Nanocomposite.** The XRD analysis revealed the presence of  $\text{CeO}_2$  and  $\text{Sm}_2\text{O}_3$  with a single-phase present in the prepared sample (Figure 1). The crystallinity of  $\text{CeO}_2$  was notably high, as indicated by the

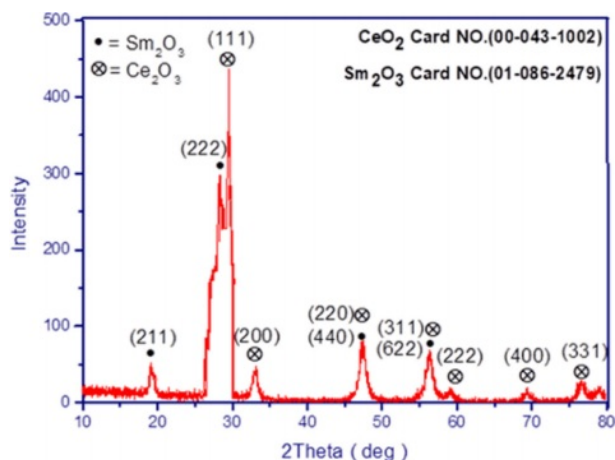


**Figure 1.** XRD patterns of CeO<sub>2</sub>/Sm<sub>2</sub>O<sub>3</sub> nanoparticle.

distinct diffraction peaks observed. The deposited films exhibited a polycrystalline structure with a cubic composition characteristic of fluorite CeO<sub>2</sub>. Specifically, common peaks were observed at  $2\theta$  angles of 29.51°, 33.13°, 59.16°, 69.39°, and 76.52°, corresponding to the (111), (200), (222), (400), and (331) orientation planes, respectively. Additionally, peaks at  $2\theta$  angles of 19.19° and 28.25° were observed, corresponding to the (211) and (222) orientation planes for Sm<sub>2</sub>O<sub>3</sub>. Notably, there were overlapping peaks at 47.36°, corresponding to (220) CeO<sub>2</sub> and (440) Sm<sub>2</sub>O<sub>3</sub>, as well as at 56.05°, which belonged to ((311) CeO<sub>2</sub> and (440) Sm<sub>2</sub>O<sub>3</sub>).

To determine the average crystalline size ( $D$ ) of the synthesized CeO<sub>2</sub>/Sm<sub>2</sub>O<sub>3</sub> nanoparticles, Scherrer's equation was applied based on (222) and (111) lattice plane peaks<sup>27,28</sup> as in the following:

$$D = \frac{k\lambda}{\beta \cos \theta} \quad (1)$$

Here, with  $k$  as the Scherrer constant ( $k = 0.9$ ),  $\lambda$  as the constant X-ray wavelength ( $\lambda = 0.1540$  nm),  $\beta$  representing the full width at half maximum in radians, and  $\theta$  as the Bragg angle, the average crystalline size ( $D$ ) of the synthesized nanoparticles was calculated to be 21.23 nm.

**Determination of Grain Size in CeO<sub>2</sub>/Sm<sub>2</sub>O<sub>3</sub> Nanoparticle.** Scanning electron microscopy (SEM) is a cutting-edge technique utilized for the analysis of surface morphology and the elucidation of the nanocomposite structure by employing an electron beam on the sample's surface. In Figure 2, the FESEM analysis of the nanomaterial surface is presented. The image vividly displays discrete clusters of nanoparticles, each exhibiting varying dimensions at the nanometer scale, with an average

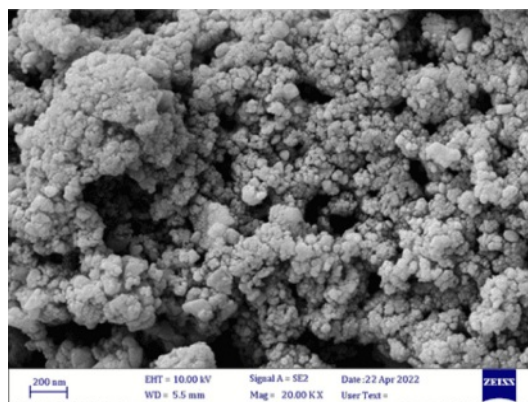


**Figure 2.** FESEM image of CeO<sub>2</sub>/Sm<sub>2</sub>O<sub>3</sub> nanoparticle.

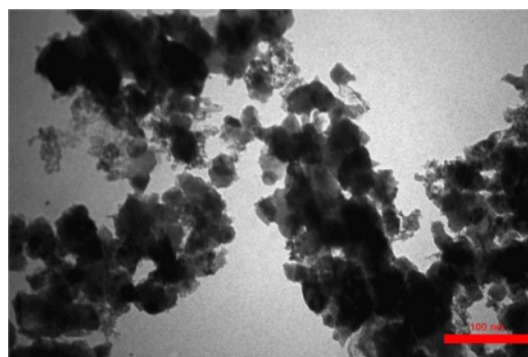


**Figure 3.** TEM image of CeO<sub>2</sub>/Sm<sub>2</sub>O<sub>3</sub> nanoparticle.

size of approximately 27 nm. Furthermore, the TEM analysis, as showcased in Figure 3, not only enhances the visualization of these nanostructures but also furnishes definitive confirmation of the presence of nanoparticles, revealing an average size of 23 nm.

**Photochemical Investigation of PVC and PVC-Nanocomposite Films via Infrared Spectroscopy.** Pure and composite PVC exhibit clear changes in its infrared spectrum when subjected to high-energy UV light at a wavelength of 365 nm (Figure 5). To understand these changes, films of additive-free PVC, with a thickness of 40  $\mu$ m, were irradiated for varying durations: 0 h, 50 h, 100 h, 200 h, and 300 h. The emergence of specific bands in the range of 1720-1775  $\text{cm}^{-1}$  is attributed to the synthesis of carbonyl groups associated with chloroketone and aliphatic ketone functionalities. Additionally, a distinct band related to the polyene group first becomes apparent at approximately 1622  $\text{cm}^{-1}$ , while a broad band appeared around 3400  $\text{cm}^{-1}$ , signifying the formation of hydroxyl groups upon prolonged irradiation. It is noteworthy that the absorption band associated with hydroxyl groups initially existed at a lower intensity prior to irradiation due to thermal oxidation

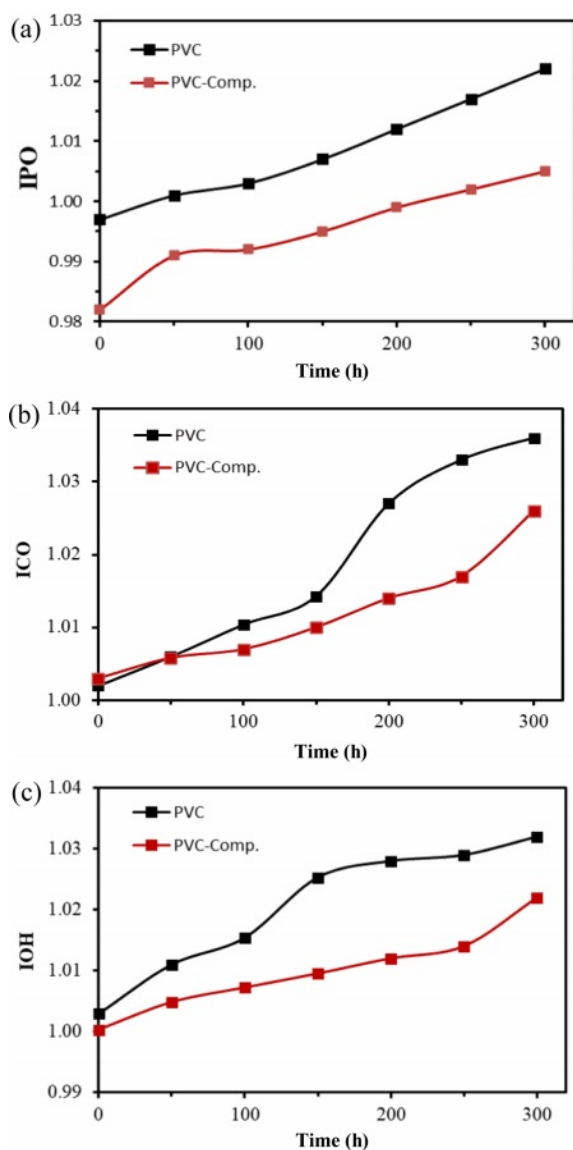


**Figure 4.** The index coefficients of (a) polyene (IPO); (b) carbonyl (ICO); (c) hydroxyl index (IOH); (d) after irradiation for 50, 100, 150, 200, 250, and 300 h.

during the PVC production process. These bands represent types of products generated during the decomposition process of PVC.<sup>8</sup>

To assess the photostabilization effectiveness of nanocomposites, they were incorporated as optical stabilizers in PVC films, enabling a comparison with films lacking these additives. Infrared spectroscopy was employed to monitor the evolution of carbonyl groups (C=O), polyene groups (C=C), and hydroxyl groups (O-H) as a function of irradiation time during the photolysis of PVC films. This monitoring allowed the determination of coefficients for hydroxyl ( $I_{OH}$ ), carbonyl ( $I_{CO}$ ), and

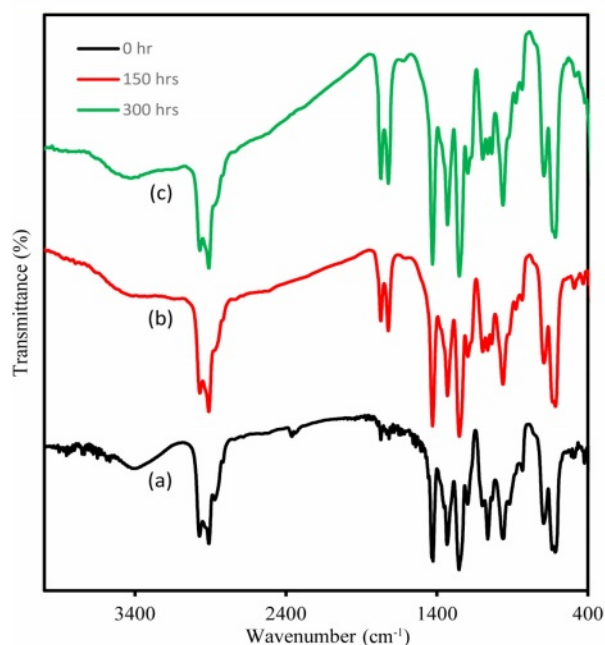


**Figure 5.** Infrared spectra of (a) PVC-CeO<sub>2</sub>/Sm<sub>2</sub>O<sub>3</sub> thin film before irradiation; (b) after 150 h; (c) and after 300 h of UV irradiation.

polyene ( $I_{PO}$ ).

The pure PVC and its composite films with a 40 micrometer thickness were observed to be decomposing increasingly as the irradiation progressed with time, resulting in an intensity increase for carbonyl ( $I_{CO}$ ), polyene ( $I_{PO}$ ), hydroxyl ( $I_{OH}$ ) indices. The following equation was used to obtain the mentioned indices.

$$I_{fun.} = A_s/A_r$$

where  $I_{fun.}$  stand for absorbance of functional groups for  $I_{OH}$ ,  $I_{PO}$ , and  $I_{CO}$ . Whereas  $A_r$  stands for the absorbance of the reference group, which is the CH<sub>2</sub> peak at 1331 cm<sup>-1</sup>.

The results indicate the effect of the additives' presence in slowing down the increment rate of all peaks of the three coefficient indices in comparison with the absence of the additives in the PVC films. This observation signifies that the additives effectively reduced the decomposition of PVC films, thereby functioning as optical stabilizers. These findings align with prior research, highlighting the role of stabilizers in decreasing the rate of PVC fragmentation.<sup>29</sup>

**Determination of Stabilizing Efficiency through Weight Loss.** The effectiveness of stabilization was assessed by measuring the weight loss percentage during the photodegradation of PVC films, both in the absence and presence of additives. Weight loss was quantified using the following equation:<sup>30</sup>

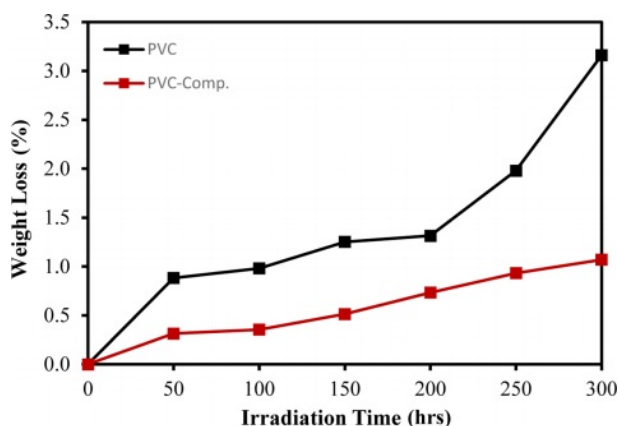


**Figure 6.** Weight loss of prepared film after irradiation for 50, 100, 150, 200, 250, and 300 h.

$$\text{Weight loss\%} = \frac{w_1 - w_2}{w_1} \times 100$$

where  $w_1$  represents the weight of the original sample before irradiation, while  $w_2$  represents the weight of the sample after irradiation.

The photodegradation of PVC results in the loss of hydrogen chloride, leading to an increase in weight loss with prolonged irradiation. Therefore, the percentage of weight loss serves as an indicator of irradiation time and can effectively measure the extent of decomposition. This metric provides insights into the stabilizer's ability to maintain the polymer's stability and protect it from degradation.<sup>31</sup> The pure PVC exhibited the highest weight loss after irradiation for 300 h, as illustrated in Figure 6. The PVC-CeO<sub>2</sub>/Sm<sub>2</sub>O<sub>3</sub> thin film, however, showed a steady and lowest increase in the weight loss in comparison to the pure PVC.

**Microscopic Images of PVC and PVC-CeO<sub>2</sub>/Sm<sub>2</sub>O<sub>3</sub> Thin Film.** Microscopic examination of thin films composed of PVC-CeO<sub>2</sub>/Sm<sub>2</sub>O<sub>3</sub> and pure PVC provided valuable insights into their surface characteristics. Figure 7(a, b) displays the surface morphology of the pure polymer and nanocomposite thin films before irradiation. In contrast, Figure 7(c, d) presents the microscopic images after irradiation. The micrographs reveal that the polymers infused with nanomaterials exhibited minimal changes, indicating the additives' effectiveness in preserving the polymeric films and functioning as optical stabilizers. In contrast, the pure polymer displayed multiple holes on its surface, signifying degradation.<sup>32</sup>

**AFM Images for PVC and PVC-Nanocomposite Thin Films.** Figure 8(a) illustrates the appearance of pure PVC prior to the irradiation process. The thin film of pure PVC features

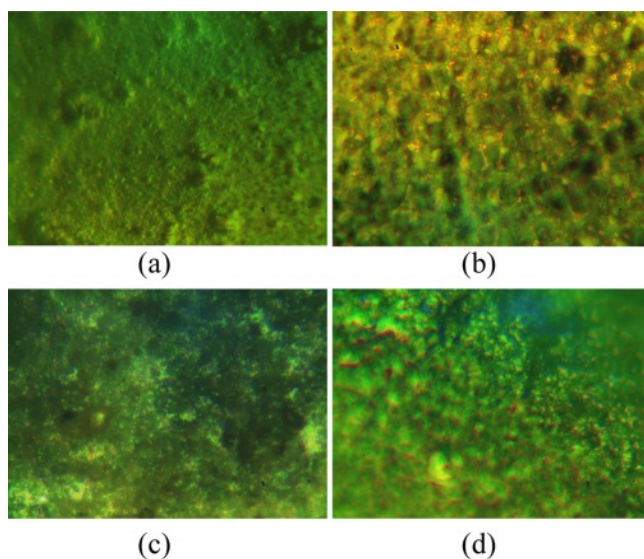


**Figure 7.** Microscopic images of (a) PVC; (b) and PVC-CeO<sub>2</sub>/Sm<sub>2</sub>O<sub>3</sub> thin film; (c) before irradiation; (d) after irradiation for 300 h.

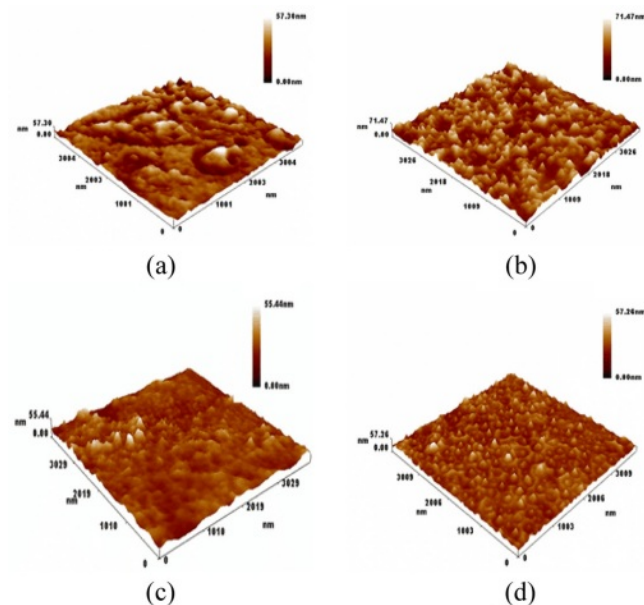


**Figure 8.** Microscopic images of (a) PVC; (b) PVC-CeO<sub>2</sub>/Sm<sub>2</sub>O<sub>3</sub> thin film; (c) before irradiation as well as PVC; (d) PVC-CeO<sub>2</sub>/Sm<sub>2</sub>O<sub>3</sub> thin film after irradiation for 300 h.

agglomerates of granules depicted as planar groups, with a measured roughness of 6.77 nm and an root mean square (RMS) value of 8.65 nm. Figure 8(b) presents the aggregated PVC with nano-granules, with white microspheres representing pores. This configuration yields a roughness of 7.36 nm and an RMS of 8.39 nm. Figure 8(c) and (d) portray the PVC and PVC-nanocomposite films after 300 h of radiation. In these images, the

**Table 1. The Average Roughness (nm) and RMS (nm) of PVC and PVC Thin Film Before and After Irradiation**

Material	Roughness average (nm)	Root mean square of roughness RMS (nm)
PVC before irradiation	6.77	8.65
PVC thin film before irradiation	7.36	8.39
PVC after irradiation for 300 h	2.99	4.26
PVC thin film after irradiation for 300 h	3.19	4.98

PVC matrix is shown to contain pores and grains gathered on the picture plane, with a roughness of 2.99 nm and an RMS of 4.26 nm. Figure 8(d) exhibits densely packed nanopore granules and pores that entirely cover the PVC matrix, resulting in a roughness of 3.19 nm and an RMS of 4.98 nm. These observations underscore the notable roughness of nanocomposite thin films, as detailed in Table 1.

## Conclusions

Incorporating nanomaterials, characterized by their high surface area and straightforward synthesis, emerges as a successful strategy for extending polymer longevity and shielding them from solar-induced degradation. Nanomaterials offer an appealing alternative to conventional microscopic additives. This study utilized a commercially available nanomaterial with a relatively large nanoscale size, demonstrating its efficacy in enhancing polymer stability. The results convincingly show that the prepared films remain resilient to environmental factors, such as light and heat, as evidenced by a reduced average weight loss percentage and reinforced by measurements of polyene ( $I_{PO}$ ), hydroxyl ( $I_{OH}$ ) and carbonyl ( $I_{CO}$ ) indices. The addition of nanomaterials proves ideal for long-term polymer stability, protecting against ultraviolet radiation, peroxide decomposition, and radical scavenger mechanisms. This research contributes to the growing understanding of nanomaterials' potential in polymer protection, with implications for various industries reliant on polymer-based materials, from packaging to electronics.

**Acknowledgment:** The authors would like to thank Mustansiriyah University ([www.uomustansiriyah.edu.iq](http://www.uomustansiriyah.edu.iq)) Baghdad-Iraq for supporting the present work.

**Conflict of Interest:** The authors declare that there is no conflict of interest.

## References

- Wilkes, C. E.; Summers, J. W.; Daniels, C. A.; Berard, M. T. *PVC handbook*; Hanser: Munich, 2005.
- Gupta, V. K.; Singh, A. K.; Mehtab, S.; Gupta, B. A. Cobalt (II)-selective PVC Membrane Based on a Schiff Base Complex of N,N'-bis (salicylidene)-3,4-diaminotoluene. *Anal. Chim. Acta* **2006**, 566, 5-10.
- Ye, Q.; Ma, X.; Li, B.; Jin, Z.; Xu, Y.; Fang, C.; Zhou, X.; Ge, Y.; Ye, F. Development and Investigation of Lanthanum Sulfadiazine with Calcium Stearate and Epoxidised Soyabean Oil as Complex Thermal Stabilizers for Stabilizing Poly(vinyl chloride). *Polymers* **2019**, 11, 531.
- Jin, D.; Khanal, S.; Zhang, C.; Xu, S. Photodegradation of Polybenzimidazole/polyvinyl Chloride Composites and Polybenzimidazole: Density Functional Theory and Experimental Study. *J. Appl. Polym. Sci.* **2021**, 138, 49693.
- Sivalingam, G.; Karthik, R.; Madras, G. Effect of Metal Oxides on Thermal Degradation of Poly(vinyl acetate) and Poly(vinyl chloride) and Their Blends. *Ind. Eng. Chem. Res.* **2003**, 42, 3647-3653.
- Taha, T.; Hendawy, N.; El-Rabaie, S.; Esmat, A.; El-Mansy, M. Effect of NiO NPs Doping on the Structure and Optical Properties of PVC Polymer Films. *Polym. Bull.* **2019**, 76, 4769-4784.
- Al-Sarray, A. Advancements in Conjugated Polymer Research: Applications in Organic Photovoltaics and Field Effect Transistors. *Curr. Chem. Lett.* **2024**, 13, 207-224.
- Lu, T.; Solis-Ramos, E.; Yi, Y.; Kumosa, M. Particle Removal Mechanisms in Synergistic Aging of Polymers and Glass Reinforced Polymer Composites Under Combined UV and Water. *Compos. Sci. Technol.* **2017**, 153, 273-281.
- Ma, Y.; Liao, S.; Li, Q.; Guan, Q.; Jia, P.; Zhou, Y. Physical and Chemical Modifications of Poly(vinyl chloride) Materials to Prevent Plasticizer Migration-still on the Run. *React. Funct. Polym.* **2020**, 147, 104458.
- Kameda, T.; Ono, M.; Grause, G.; Mizoguchi, T.; Yoshioka, T. Ball Mill-assisted Dechlorination of Flexible and Rigid Poly(vinyl chloride) in NaOH/EG Solution. *Ind. Eng. Chem. Res.* **2008**, 47, 8619-8624.
- Braun, D. Poly(vinyl chloride) on the Way From the 19th Century to the 21st Century. *J. Polym. Sci. Part A: Polym. Chem.* **2004**, 42, 578-586.
- Keane, M. A. Catalytic Conversion of Waste Plastics: Focus on Waste PVC. *J. Chem. Technol. Biotechnol. International Research in Process, Environ. Clean Technol.* **2007**, 82, 787-795.
- Hajibeygi, M.; Maleki, M.; Shabani, M.; Ducos, F.; Vahabi, H. New Polyvinyl Chloride (PVC) Nanocomposite Consisting of Aromatic Polyamide and Chitosan Modified ZnO Nanoparticles with Enhanced Thermal Stability, Low Heat Release Rate and Improved Mechanical Properties. *Appl. Surf. Sci.* **2018**, 439, 1163-1179.
- Cho, S.; Choi, W. Solid-phase Photocatalytic Degradation of PVC-TiO<sub>2</sub> Polymer Composites. *J. Photochem. Photobiol. A* **2001**, 143, 221-228.

15. Wang, M.; Wu, T.; Bu, Q.; Song, X.; Li, M.; Yuan, S. Rare Earth Ce Based Metal Organic Framework as Efficient Synergistic Thermal Stabilizer for PVC: Preparation and Thermal Stabilization Behavior. *Thermochim. Acta* **2022**, 718, 179365.
16. Li, M.; Jiang, Z.; Liu, Z.; Hu, Y.; Wang, M.; Wang, H. Effect of Lanthanum Cyanurate as Novel Organic Thermal Stabilizers for Polyvinyl Chloride. *Polym. Eng. Sci.* **2013**, 53, 1706-1711.
17. Xie, L.; Li, D.; Fu, M.; Zhang, J.; Zhang, L.; Zhang, Y.; Zhao, P. Study on Lanthanum-pentaerythritol Alkoxide as a Thermal Stabilizer for Rigid Polyvinyl Chloride. *J. Vinyl Addit. Technol.* **2017**, 23, 55-61.
18. Jasim, B. E.; Al-Sarray, A. J. and Dadoosh, R. M. Enhanced Alizarin Removal from Aqueous Solutions Using Zinc Oxide/Nickel Oxide Nano-composite. *Anal. Sci. Technol.* **2024**, 37, 39-46.
19. Liu, J.; Dai, M.; Wang, T.; Sun, P.; Liang, X.; Lu, G.; Shimanoe, K.; Yamazoe, N. Enhanced Gas Sensing Properties of SnO<sub>2</sub> Hollow Spheres Decorated with CeO<sub>2</sub> Nanoparticles Heterostructure Composite Materials. *ACS Appl. Mater. Interfaces* **2016**, 8, 6669-6677.
20. Al-Sarray, A. J. A. Molecular and Electronic Properties of Schiff Bases Derived from Different Aniline Derivatives: Density Functional Theory Study. *Eurasian Chem. Commun.* **2023**, 5, 317-326.
21. Sykora, R. E.; Deakin, L.; Mar, A.; Skanthakumar, S.; Soderholm, L.; Albrecht-Schmitt, T. E. Isolation of Intermediate-Valent Ce (III)/Ce(IV) Hydrolysis Products in the Preparation of Cerium Iodates: Electronic and Structural Aspects of Ce<sub>2</sub>(IO<sub>3</sub>)<sub>6</sub> (OH)<sub>x</sub> (x≈0 and 0.44). *Chem. Mater.* **2004**, 16, 1343-1349.
22. Kalinina, M.; Dyuskina, D.; Fedorenko, N. Y.; Shilova, O. Effect of Liquid-Phase Synthesis Method of Nanopowders on Microstructure and Physicochemical Properties of Ceramics in CeO<sub>2</sub>-Sm<sub>2</sub>O<sub>3</sub> System. *Inorg. Mater. Appl. Res.* **2022**, 13, 501-507.
23. Dědková, K.; Kuzníková, L.; Pavelek, L.; Matějová, K.; Kupková, J.; Barabaszová, K. Č.; Váňa, R.; Burda, J.; Vlček, J.; Cvejn, D. Daylight Induced Antibacterial Activity of Gadolinium Oxide, Samarium Oxide and Erbium Oxide Nanoparticles and Their Aquatic Toxicity. *Mater. Chem. Phys.* **2017**, 197, 226-235.
24. Dhamodharan, K.; Singh, A. K. Highly Performed Electrochemical Activities of Hybrid Supercapacitors Based on CeO<sub>2</sub>-Sm<sub>2</sub>O<sub>3</sub> Nanocomposites. *Electrochim. Acta* **2023**, 466, 143008.
25. Saraci, F.; Quezada-Novoa, V.; Donnarumma, P. R.; Howarth, A. J. Rare-earth Metal-organic Frameworks: from Structure to Applications. *Chem. Soc. Rev.* **2020**, 49, 7949-7977.
26. Al-Sarray, A. J.; H. Al-Mousawi, I. M.; H. Al-Noor, T. Acid Activation of Iraqi Bentonite Clay: Its Structural, Dielectric and Electrical Behavior at Various Temperatures. *Chem. Methodol.* **2022**, 6, 331-338.
27. Chibac-Scutaru, A. L.; Podasca, V.; Dascalu, I. A. and Melinte, V. Exploring the Influence of Synthesis Parameters on the Optical Properties for Various CeO<sub>2</sub> NPs. *Nanomaterials* **2022**, 12, 1402.
28. Joseph, A.; Ayyappan, A.; Subair, T.; Pandibayal, M.; Nair, S.; Ramany, R.; Raama Varma, M. and Thomas, S. Pure and Sm Doped CeO<sub>2</sub> Nanoparticles: An Insight Into the Room Temperature Ferromagnetism and Photocatalytic Dye Degradation. *Chemistry Select* **2023**, 8, e202301020.
29. Al-Tikrity, E. T.; Yaseen, A. A.; Yousif, E.; Ahmed, D. S. and Al-Mashhadani, M. H. Impact on Poly(Vinyl chloride) of Trimethoprim Schiff Bases as Stabilizers. *Polym. Polym. Compos.* **2022**, 30, 09673911221094020.
30. Jafari, A. J.; Donaldson, J. D. Determination of HCl and VOC Emission from Thermal Degradation of PVC in the Absence and Presence of Copper, Copper (II) Oxide and Copper (II) Chloride. *E-J. Chem.* **2009**, 6, 685-692.
31. Pospíšil, J. and Nešpurek, S. Photostabilization of Coatings. Mechanisms and Performance. *Prog. Polym. Sci.* **2000**, 25, 1261-1335.
32. El-Hiti, G. A.; Alotaibi, M. H.; Ahmed, A. A.; Hamad, B. A.; Ahmed, D. S.; Ahmed, A.; Hashim, H.; Yousif, E. The Morphology and Performance of Poly(vinyl chloride) Containing Melamine Schiff Bases Against Ultraviolet Light. *Molecules* **2019**, 24, 803.

**Publisher's Note** The Polymer Society of Korea remains neutral with regard to jurisdictional claims in published articles and institutional affiliations.